Supplementary data

Anisotropic Nanoparticles of Precise Microstructure Polyolefins

Justyna Trzaskowski, Marina Krumova and Stefan Mecking

University of Konstanz, Chair of Chemical Materials Science, Department of Chemistry,78464 Konstanz (Germany). E-mail: stefan.mecking@uni-konstanz.de

Christian Rabe, Karsten Vogtt, Guenter Goerigk and Matthias Ballauff

Helmholtz–Zentrum Berlin for Materials and Energy, Hahn Meitner-Platz 1, D-14109 Berlin (Germany). E-mail: matthias.ballauff@helmholtz-berlin.de

Materials and General Considerations. Unless noted otherwise, all manipulations were carried out under an inert gas atmosphere using standard glovebox or Schlenk techniques. Toluene was distilled from sodium under argon prior to use. All other solvents were utilized in technical grade as received unless noted otherwise. Distilled water was degassed by saturation with nitrogen. Benzylidenebis(tricyclohexylphosphine)dichlororuthenium, ethyl vinyl ether and dodecyltrimethylammonium chloride (DTAC) were supplied by Sigma Aldrich. NMR spectra were recorded on a Varian Unity INOVA 400 instrument. ^{1}H and ^{13}C NMR chemical shifts were referenced to the solvent signal. GC analysis was carried out on a Perkin Elmer Clarus 500 GC system equipped with a Perkin Elmer Elite-5 capillary column (30 m × 0.25 mm × 0.25 µm, 5% diphenyl - 95% dimethyl polysiloxane) using flame ionization detection. Helium of 99.995% purity was used as the carrier gas. The initial temperature of 90°C was kept for one minute, and the column was then heated at a rate of 30 K min^{-1} to 280°C, and kept isothermal at this temperature for 8 min (injector temperature 300°C; detector temperature 280°C). Differential scanning calorimetry (DSC) was performed on a Netzsch Phoenix 204 F1 at a heating/cooling rate of 10 K min^{-1}. DSC data reported are from second heating cycles, unless noted otherwise. Gel permeation chromatography (GPC) was carried out on a Polymer Laboratories PL-GPC 50 with two PLgel 5 µm MIXED-C columns and a RI-detector in THF at 40°C against polystyrene standards. Dynamic light scattering (DLS) on diluted latex samples was performed on a Malvern Nano-ZS ZEN 3600 particle sizer (173° back scattering). The autocorrelation function was analyzed using the Malvern dispersion technology zetasizer software 6.2 to obtain volume, number and intensity weighted particle size distributions. TEM investigations were performed on a Zeiss Libra 120 transmission electron microscope operated at120 kV acceleration voltage. Samples were prepared by applying a drop of the latex to a carbon coated grid.

Monomer synthesis. The α,ω-dienes **1** and **2** used in this work were synthesized according to the literature procedure reported by Wagener and co-workers.[10] Purity from GC: > 99%.

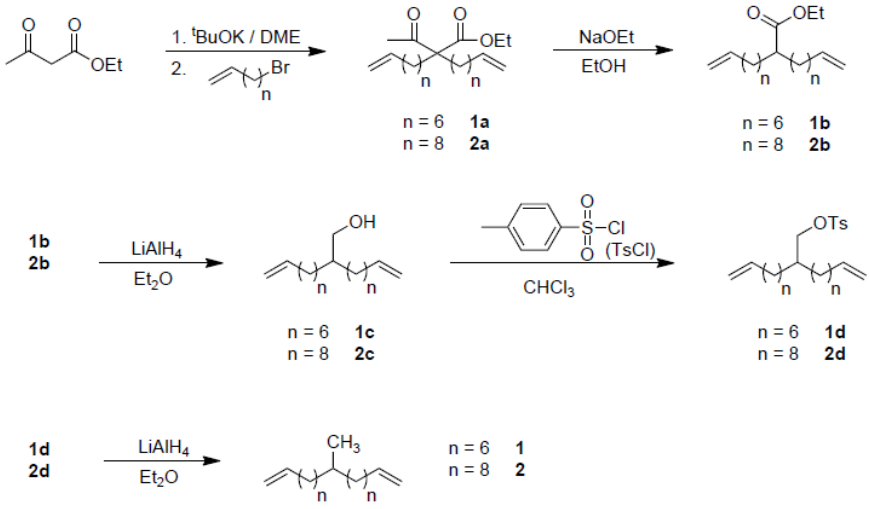

Fig. S1 Synthetic approach for the preparation of monomers **1** and **2**.[10]

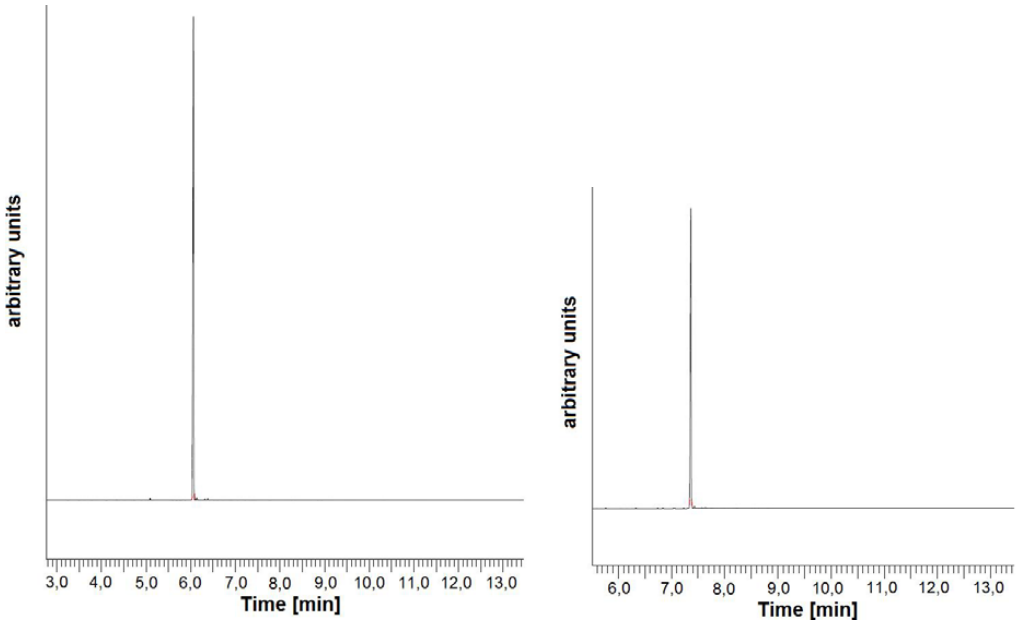

Fig. S2 Gas chromatogram of monomer **1** (left) and **2** (right) (5% diphenyl - 95% dimethylpolysiloxane column; 90°C isothermal for 1 min, 30 K min^{-1} to 280°C, isothermal for 8 min).

Polymerizations were carried out in a 100 mL mechanically stirred Schlenk tube equipped with a vacuum adapter. To the monomer in the Schlenk tube (**1**: 4.06 g, 16.2 mmol; **2**: 4.85 g, 15.9 mmol) Grubbs 1st generation catalyst, dissolved in 2.0 ml of toluene, (for polymerization of: **1**: 28.2 mg, 34.3 µmol; **2**: 26.8 mg, 32.6 µmol) was added under vigorous stirring. The reaction mixture was stirred at RT for 15 min. and then at 0.025 mbar until toluene evaporation ceased. The further polymerization was performed at 50°C and 0.025 mbar for six days to obtain a brownish, highly viscous polymer in quantitative yield.

NMR analysis of poly-**1**:

^{1}H NMR (400 MHz, $CDCl_3$, 25 °C, δ): 5.79 (m, **H**C=CH_2 endgroup), 5.36 + 5.33 (trans + cis, m, 2H, **H**C=C**H**, **e**), 4.94 (m, HC=C**H**$_2$ endgroup), 1.95 (m, 4H, CH=CHC**H**$_2$, **f**), 1.24 - 1.06 (m, 29H, C**H**$_2$, **c**, **d**, **g**, **h**, C**H**CH_3), 0.86 (t, *J* = 6.7 Hz, C**H**$_3$ endgroup), 0.82 (d, *J* = 6.4 Hz, 3H, C**H**$_3$ branch, **a**); ^{13}C NMR (100 MHz, $CDCl_3$, 25°C, δ): 130.50 + 130.04 (trans + cis **e**), 37.28 (**c**), 32.93 (**f**), 32.80 (**b**), 30.06 (**g**), 29.95, 29.86, 29.54, 29.41, 27.39 (**h**), 27.34 (**d**), 19.87 (**a**).

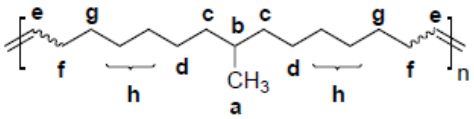

NMR analysis of poly-**2**:

^{1}H NMR (400 MHz, $CDCl_3$, 25 °C, δ): 5.79 (m, **H**C=CH_2 endgroup), 5.37 + 5.33 (trans + cis, m, 2H, **H**C=C**H**, **e**), 4.95 (m, HC=C**H**$_2$ endgroup), 1.96 (m, 4H, CH=CHC**H**$_2$, **f**), 1.25 - 1.05 (m, 29H, C**H**$_2$, **c**, **d**, **g**, **h**, C**H**CH_3, **b**), 0.86 (t, *J* = 6.7 Hz, C**H**$_3$ endgroup), 0.83 (d, *J* = 6.4 Hz, 3H, C**H**$_3$ branch, **a**); ^{13}C NMR (100 MHz, $CDCl_3$, 25°C, δ): 130.59 + 130.11 (trans + cis **e**), 37.35 (**c**), 33.00 (**f**), 32.87 (**b**), 30.13 (**g**), 30.03, 29.93, 29.61, 29.48, 27.46 (**h**), 27.31 (**d**), 19.95 (**a**).

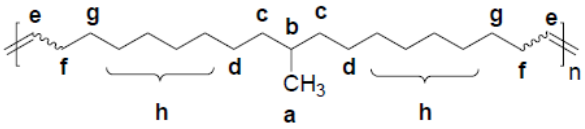

Secondary dispersion. The unsaturated polymer (poly-**1**: 128.5 mg; poly-**2**: 127.4 mg) was dissolved in 8.0 ml of toluene. A 0.8 wt% DTAC solution was placed in a 100 ml Schlenk flask. The polymer solution was added to the surfactant solution under ultrasonication. Ultrasonication was performed for 25 min. under a continuous flow of argon. Dynamic light scattering (DLS) on the dispersion revealed an average particle size of 25 nm for poly-**1** and 35 nm for poly-**2**. (Bandelin HD 3200 Sonoplus ultrasonotrode with a KE76 tip was employed).

Hydrogenation in secondary dispersion. Grubbs' 1st generation catalyst (41.8 mg for poly-**1**, 42.9 mg for poly-**2**) was dissolved in 2.0 ml of toluene and 1.0 ml ethyl vinyl ether was added. The reaction mixture was stirred for 2.5 h at 50°C. In the course of the quenching reaction the deeply purple solution turned brown, indicating the formation of the fisher type carbene. The quenched catalyst was added to the polymer dispersion and the reaction mixture was transferred into an autoclave. Hydrogenation was performed at a hydrogenation pressure of 60 bar at 65°C for two days. After hydrogenation the dispersion was passed through a paper filter and stirred open to air over night to remove volatile organic solvents. Dynamic light scattering (DLS) on the dispersion revealed an average particle size of 25 nm for poly-**1**-hyd and 35 nm for poly-**2**-hyd. (Bandelin HD 3200 Sonoplus ultrasonotrode with a KE76 tip was employed). An aliquot of the dispersion was poured into 100 ml of methanol, whereupon the polymer precipitated. The polymer was filtrated, washed with methanol and dried in vacuo.

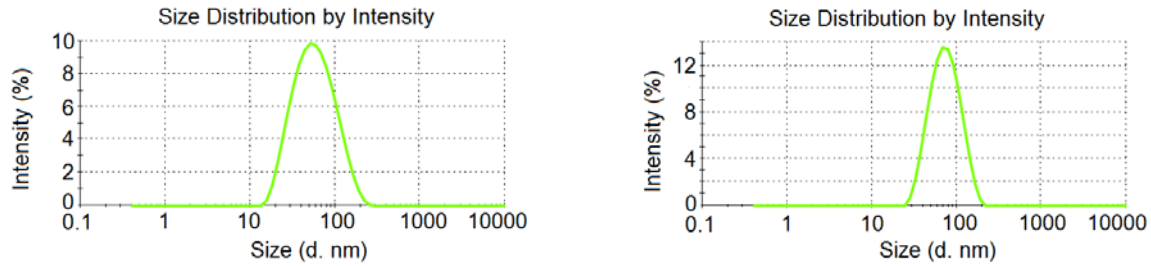

Fig. S3 Particle size distribution by intensity of poly-**1** secondary dispersion before (left, 65 nm) and after (right, 61 nm) hydrogenation.

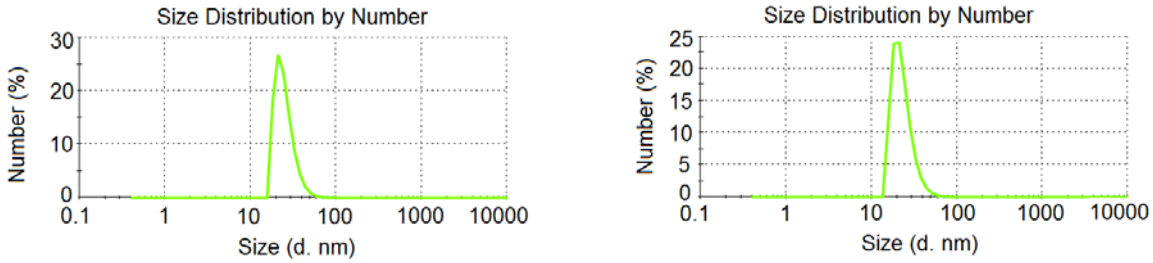

Fig. S4 Particle size distribution by number of poly-**1** secondary dispersion before (left, 25 nm) and after (right, 23 nm) hydrogenation.

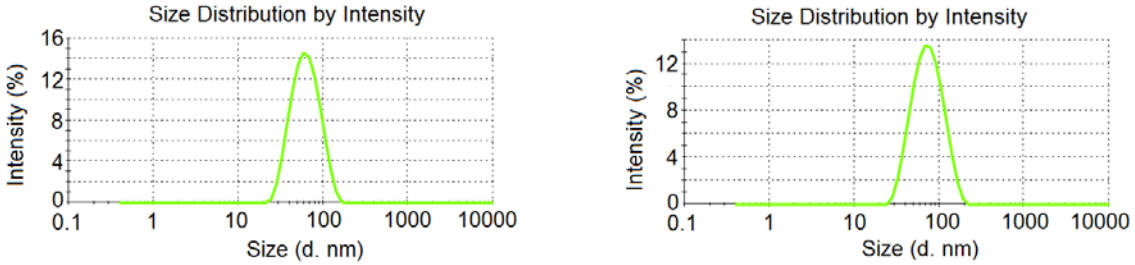

Fig. S5 Particle size distribution by intensity of poly-**2** secondary dispersion before (left, 65 nm) and after (right, 78 nm) hydrogenation.

NMR analysis of hydrogenated polymer **C15**:

^{1}H NMR (400 MHz, $CDCl_3$, 25 °C, δ): 1.22 - 1.06 (m, 37H, C**H**$_2$, **c**, **d**, **e**, **f**, C**H**CH_3, **b**), 0.85 (t, J = 6.7 Hz, C**H**$_3$ end group), 0.82 (d, J = 6.4 Hz, 3H, C**H**$_3$ branch, **a**); ^{13}C NMR (100 MHz, $CDCl_3$, 25°C, δ): 37.25 (**c**), 32.90 (**b**), 30.19 (**e**), 29.86 (**f**), 27.24 (**d**), 19.87 (**a**).

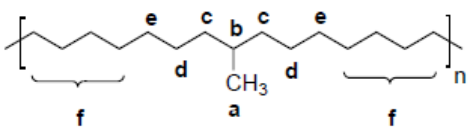

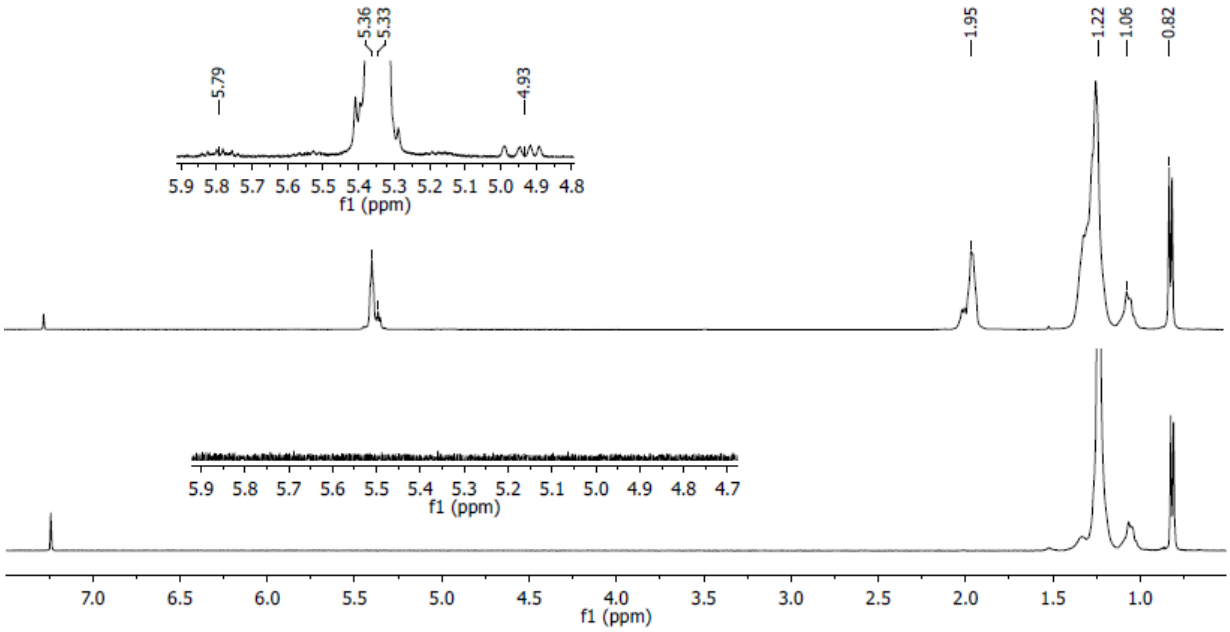

Fig. S6 ^{1}H NMR spectra (25°C, $CDCl_3$) of poly-**1** (top) and saturated polymer **C15** (bottom).

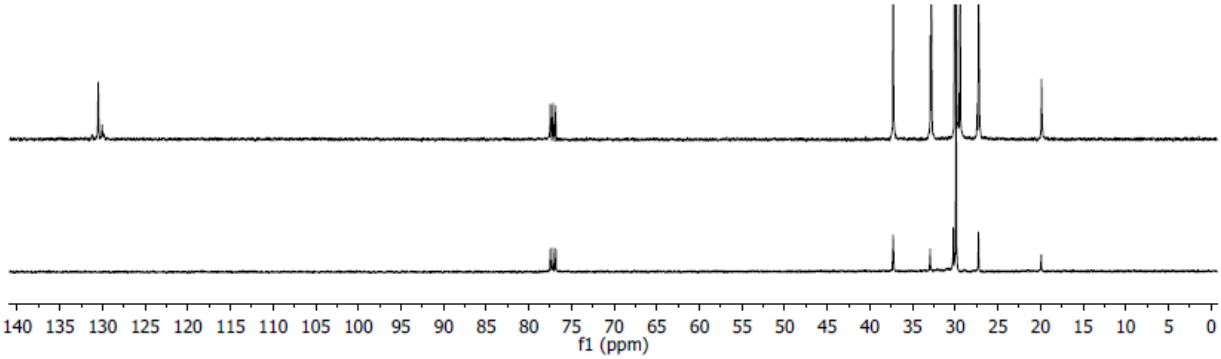

Fig. S7 ^{13}C NMR spectra (25°C, $CDCl_3$) of poly-**1** (top) and saturated polymer **C15** (bottom).

NMR analysis of hydrogenated polymer **C19**:

^{1}H NMR (400 MHz, $CDCl_3$, 25 °C, δ): 1.25 - 1.05 (m, 37H, C**H**$_2$, **c**, **d**, **e**, **f**, C**H**CH_3, **b**), 0.86 (t, J = 6.7 Hz, C**H**$_3$ end group), 0.83 (d, J = 6.4 Hz, 3H, C**H**$_3$ branch, **a**); ^{13}C NMR (100 MHz, $CDCl_3$, 25°C, δ): 37.29 (**c**), 32.94 (**b**), 30.23 (**e**), 29.90 (**f**), 27.28 (**d**), 19.91 (**a**).

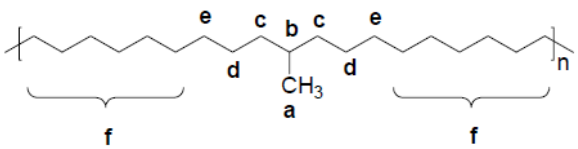

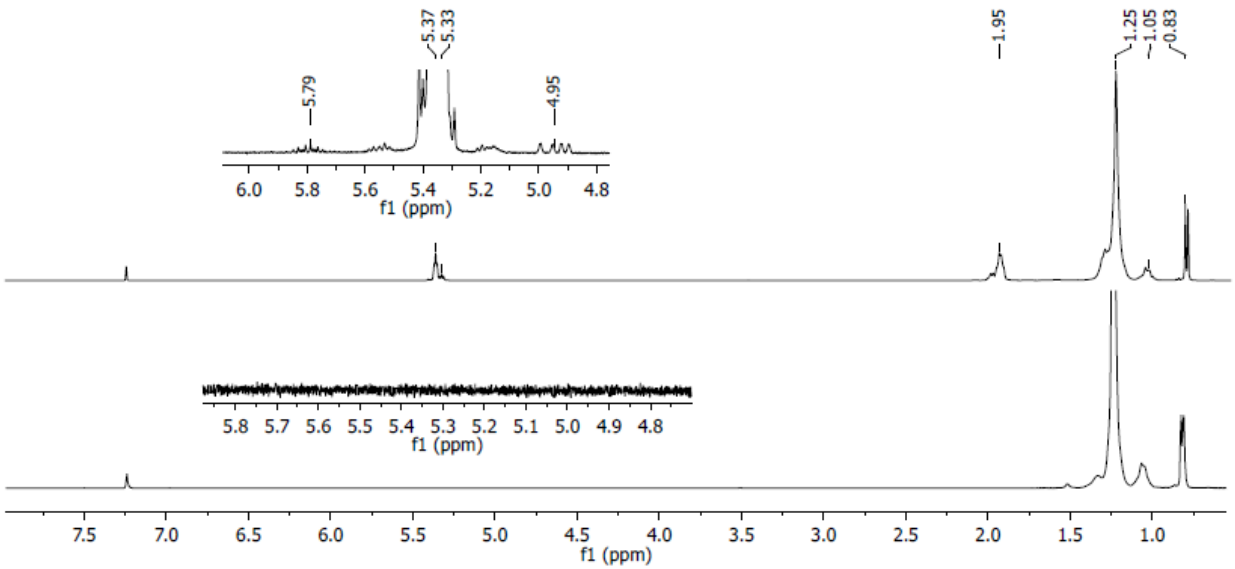

Fig. S8 ^{1}H NMR spectra (25°C, $CDCl_3$) of poly-**2** (top) and saturated polymer **C19** (bottom).

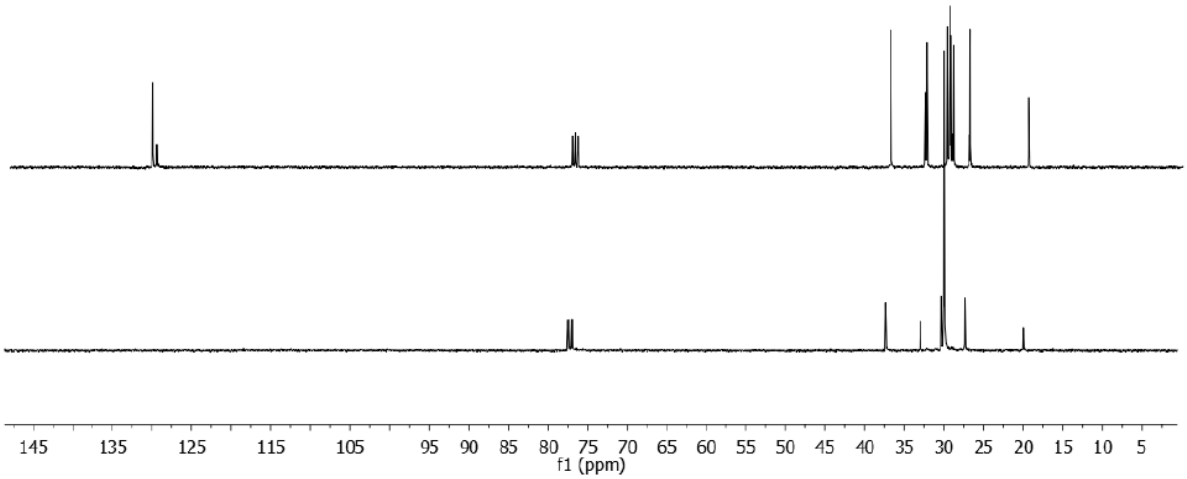

Fig. S9 ^{13}C NMR spectra (25°C, $CDCl_3$) of poly-**2** (top) and saturated polymer **C19** (bottom).

Differential scanning calorimetry (DSC). Melt enthalpies of bulk material are ΔH_m = 121 J g^{-1} for polymer **C19** and ΔH_m = 90 J g^{-1} for polymer **C15**, taken from the second heating cycle.

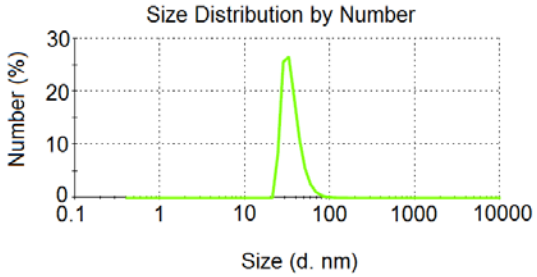

Fig. S10 DLS trace of a nanoparticle dispersion **C15-NP** after five melting and recrystallization cycles (36 nm).

Small angle x-ray scattering was performed at the ID02 beamline at ESRF in Grenoble (France). The scattering intensities were measured with a 2D FReLoN Kodak CCD detector at 2m detector position covering a q-range of $0.05<q<2.9\text{nm}^{-1}$. The photon energy was set to 12.46keV corresponding to a wavelength of λ=1Å. The samples were measured in a tempered polycarbonate flow capillary at 25°C. The acquisition time per photon shot was 100µs. For every sample ten single measurements were performed and averaged during the data reduction process. To prevent radiation damages the sample was automatically pushed stepwise through the capillary. The data reduction was performed with the software package *SAXSutilities* by Sztucki.

For the contrast variation series the following samples with **C19-NP** and the respective background solutions containing corresponding concentrations of glucose were prepared. The polymer dispersions and sugar solutions contained 1.5wt% dodecyltrimethylammonium chloride (DTAC) as stabilizing surfactant. A reduction of the surfactant content was not possible, as this was found to comprise colloidal stability.

Table S1 Overview of the composition of **C19-NP** samples of the contrast variation series. (ω_{glucose} – weight fraction glucose, $\omega_{\text{C19-NP}}$ - weight fraction **C19-NP**, $\phi_{\text{C19-NP}}$ – volume fraction **C19-NP**, ρ_m – x-ray scattering length density of dispersion medium).

sample	$\omega_{glucose}$	$\omega_{C19\text{-}NP}$	$\phi_{C19\text{-}NP}$	ρ_m
	wt%	wt%		10^{10}cm^{-2}
C19-NP 0wt% glucose	0	0.96	0.01069	9.42
C19-NP 4.5wt% glucose	4.5	0.96	0.01085	9.55
C19-NP 7wt% glucose	7	0.96	0.01096	9.63
C19-NP 15wt% glucose	15	0.96	0.01131	9.91
C19-NP 22wt% glucose	22	0.96	0.01163	10.16

The respective absolute calibrated scattering intensities as obtained from the data reduction process are shown in Fig. S11:

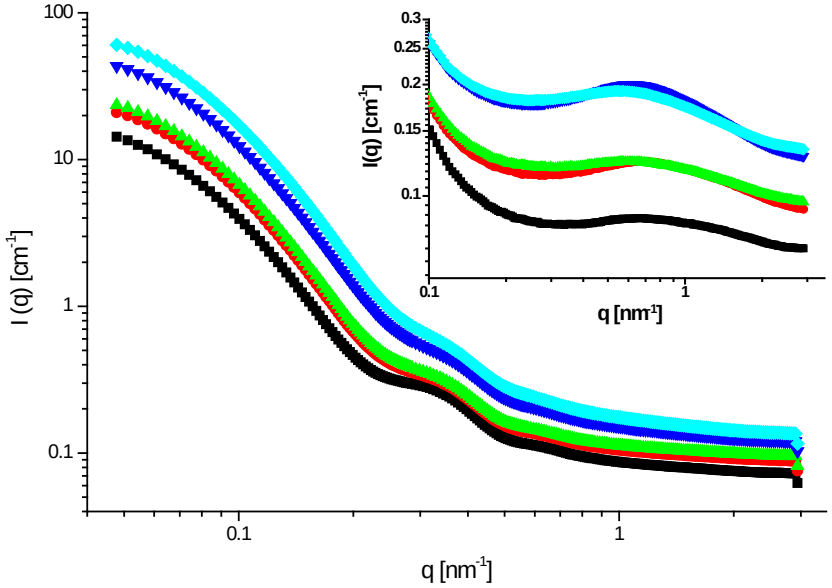

Fig. S11 Scattering intensities obtained from contrast variation series with **C19-NP** using different glucose solutions. The sugar concentration was increased from bottom to top from 0 wt%, 4.5 wt%, 7 wt%, 15 wt% to 22 wt% glucose content. The absolute calibrated data are shown without further data treatment. The inset shows the scattering intensities of the respective sugar solutions containing 1.5wt% of DTAC, as it was used in the preparation of the polymer dispersions. The symbol and colour code for the respective glucose content is the same as described for the main graph.

For the determination of the scattering contribution of the PE-nanoparticles the dispersions scattering intensities had to be corrected for the scattering intensities of the dispersing medium containing respective amounts of glucose and surfactant. In particular, the solutions contained free DTAC-micelles that contribute strongly to the scattering intensities at higher scattering angles. Thus, the weak second maxima visible around $q = 0.65\ \text{nm}^{-1}$ in the raw scattering curves had to be assigned to micelle scattering. The correction for this additional intensity was done as follows: We assume that the scattering intensity measured at different contrast is fully given by the one of the DTAC-micelles beyond $q = 1\ \text{nm}^{-1}$. The scattering intensity of a solution of DTAC-micelles at a given contrast (see inset of Fig. S11) is multiplied by an arbitrary factor until it matches the scattering

intensity of the solution of the particles in the region for q > 1nm^{-1}. This match is not perfect but sufficient to subtract the contribution of the DTAC-micelles. Fig. S12 displays the corrected intensities thus obtained. Due to the uncertainties of this subtraction, the corrected data were meaningful only for q < 0.7nm^{-1}. Hence, all subsequent analysis was restricted to this range.

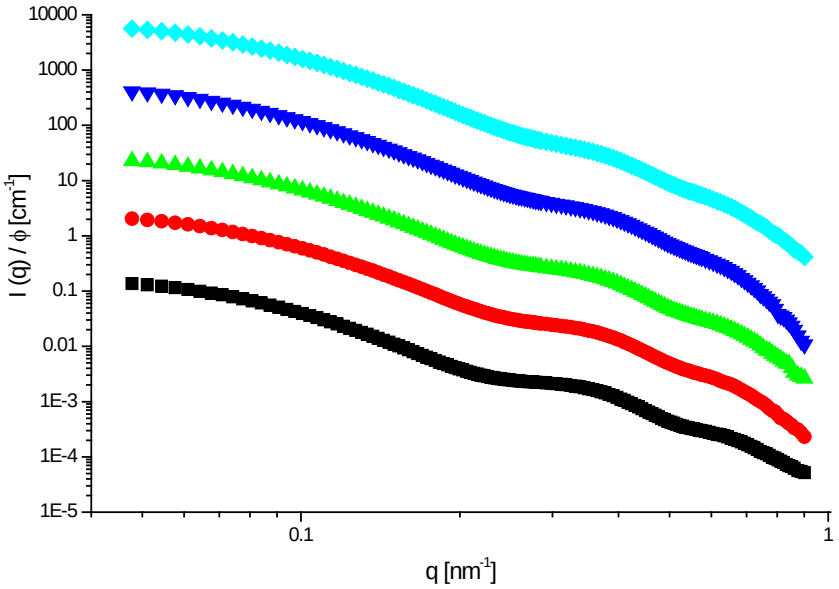

Fig. S12 Small angle scattering intensities *I(q)* of dispersions of **C19-NP** as a function of the scattering vector *q*. Intensities are background corrected and normalized to the particle volume fraction ϕ. Bottom to top: solutions with an increasing amount of added glucose (0 wt%, 4.5 wt%, 7 wt%, 15 wt% and 22 wt%). For clarity the four lower intensities were downshifted by a factor of 10, 10^2, 10^3 and 10^4, respectively.

The subsequent analysis was done as follows: The measured intensities *I(q)* of *N* particles per volume *V* can be expressed as:

$$I(q) = \frac{N}{V} I_0(q) S(q) = \phi(\Delta\rho)^2 V_P F(q) S(q) \quad (1)$$

where *q* is the scattering vector ($q=(4\pi/\lambda)\sin(\theta/2)$; λ - wavelength, θ – scattering angle) and where the intensity I_0 refers to the scattering intensity of a single particle. The interactions of the particles are described by the structure factor *S(q)*. For non-interacting particles *S(q)* becomes unity. The quantity $\Delta\rho$ denotes the contrast given by the average scattering length density of the particles ρ_P and of the surrounding medium ρ_m ($\Delta\rho=\rho_P - \rho_m$). The average particle volume is represented by V_P. The particles structure is expressed by the form factor *F(q)*.

From the analysis of the low-*q* regime by the linearised *Guinier*-equation the determination of the Scattering intensity $I(q\rightarrow 0)$ at vanishing θ and the radius of gyration R_G can be determined:

$$I(q) = I_0(q) exp\left(-\frac{(qR_G)^2}{3}\right) \quad (2)$$

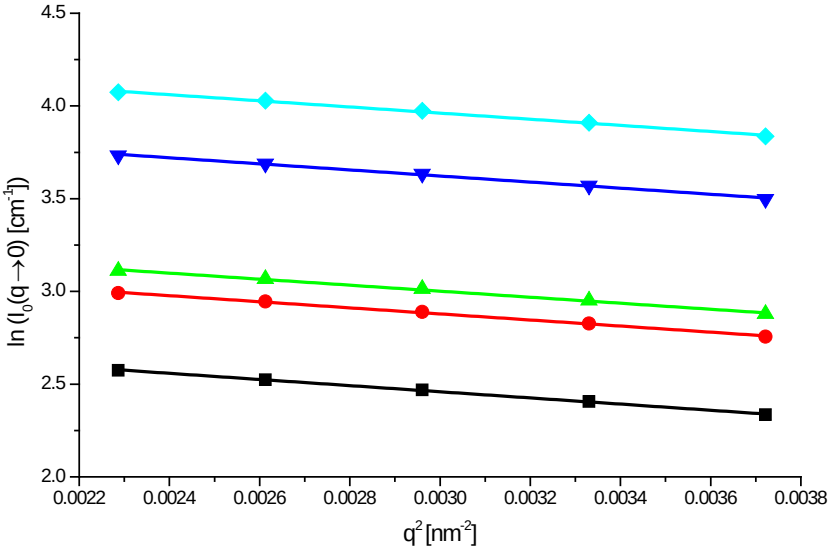

Fig. S13 *Guinier*-plots from the contrast variation series of **C19-NP** with intensities deriving from increasing ρ_m from bottom to top (0 wt%, 4.5 wt%, 7 wt%, 15 wt%, 22 wt% glucose).

The results from the Guinier-analysis are shown below (Table S2).

Table S2 Overview on the results from the *Guinier*-analysis of the low-*q* regime of scattering intensities of **C19-NP** dispersed in different solutions with glucose as contrast agent.

sample	$\omega_{glucose}$	R_G	$I_0(q \rightarrow 0)$
	wt%	Nm	cm^{-1}
C15-NP 0 wt% glucose	0	22.0 ± 2.3	18.8 ± 0.1
C15-NP 4.5 wt% glucose	4.5	22.0 ± 2.4	28.5 ± 0.1
C15-NP 7 wt% glucose	7	22.0 ± 2.4	32.2 ± 0.1
C15-NP 15 wt% glucose	15	22.1 ± 2.5	60.1 ± 0.2
C15-NP 22 wt% glucose	22	22.3 ± 2.6	85.0 ± 0.3

The approximation used therein takes into account that particle-particle interactions are negligible due to the low concentration of the polyethylene nanoparticles. The contribution of the structure factor *S(q)* on the scattering intensities *I(q)* is therefore approximated with unity.[15]

From the analysis of the scattering intensities $I(q \rightarrow 0)$ at vanishing scattering angles θ in respect of the varying scattering length density of the solvent ρ_m we extracted the average particle volume V_P from the slope of the linear fit. The average particle scattering length density ρ_P results as function of the fits intercept and the particles average volume. These amount to V_P = 36000 ± 3000 nm^3 and ρ_P = 8.71±0.04 10^{10} cm^{-2} respectively (Fig. S14).

$$\sqrt{\frac{I(q \rightarrow o)}{\phi}} = \sqrt{V_P}(\rho_P - \rho_m) \qquad (3)$$

Thus, the scattering contrast follows as $\Delta\rho = \rho_P - \rho_m$ for each solution.

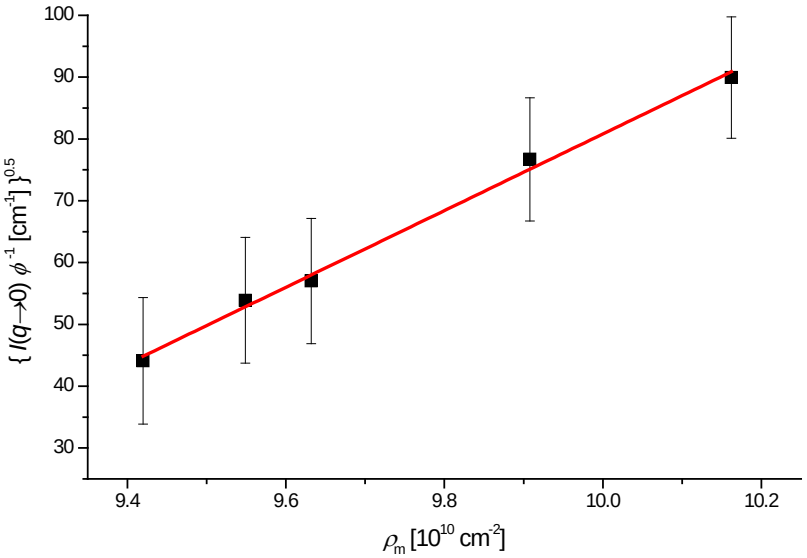

Fig. S14 The *square root*-plot allows the determination of V_P and ρ_P the correlation of the scattering intensities $I(q\rightarrow 0)$ at vanishing q-values with the scattering length density of the medium ρ_m.

The scattering intensities obtained at different contrast were decomposed according to

$$I_0(q) = I_S(q)\Delta\rho^2 + I_{SI}(q)\Delta\rho + I_I(q) \qquad (4)$$

Here $I_S(q)$ represents the shape-term describing the outer shape of the particle. $I_{SI}(q)$ is the cross-term and $I_I(q)$ refers to the inner-term that is related to the inner particle-structure. $I_S(q)$and $I_{SI}(q)$depends on the scattering contrast whereas $I_I(q)$is contrast independent. For selected q-values the volume fraction normalized scattering intensities are shown in respect to the scattering contrast in Fig. S15. This plot also shows the respective parabolic fits according to equation (4).

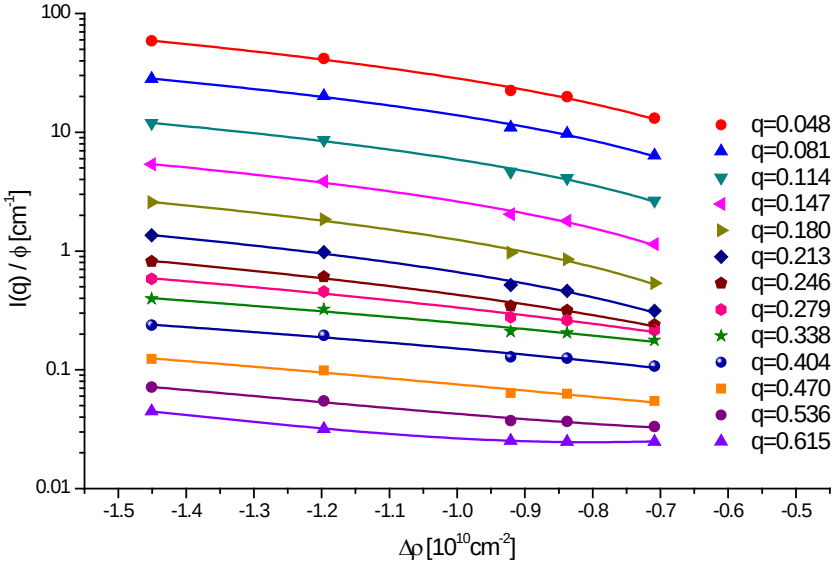

Fig. S15 Dependence of the scattering intensities I(q) of **C19NP** for selected q-values on the contrast Δρ (symbols).The parabolic fit according to equation (4) is represented by solid lines.

The fit parameters of equation (4) lead directly to the terms of $I_S(q)$, $I_I(q)$ and $I_{SI}(q)$. The algorithm works well for the q-values under consideration in Fig. S9. However, only the shape term $I_S(q)$ could be obtained securely from this extrapolation (see Fig. 4). The shape term $I_S(q)$ was modelled as an oblate-like ellipsoid (Fig. 4). The best result was obtained by a non-automated routine with the SAS evaluation software SASfit (version 0.93.3) by Kolbrecher. All attempts of an automated fitting with common geometrical models failed. The data analysis afforded $r_{eq} = 23.8 \pm 8.8$ nm for the two equatorial axis, and $r_p = 4.9 \pm 1.8$ nm for the perpendicular semi-axis. These values include a polydispersity of the semi-axis of 37%. The corresponding particles volume is $V_P = 38000\text{nm}^3$ which is within the limits of the particles volume deriving from the correlation between $I(q\rightarrow 0)$ and ρ_m. The high uncertainty used for this model was verified by electron microscopy showing

polydisperse and polymorph particles (Fig. 5). We also checked other models. The best fit for a polydisperse sphere is also plotted in the main text Fig. 4. The calculated spheres radius of $r = 13.4 \pm 5.0$ nm gives a particle volume of $V_P = 35000\text{nm}^3$. The calculated scattering intensities could not fully describe the shape term. Especially in the high-q region the model deviates significantly from the decomposed particles shape function and can be ruled out.